Nanoscale

Solution-processed organometallic quasi-two-dimensional nanosheets as hole buffer layer for organic light-emitting devices

Journal:	*Nanoscale*
Manuscript ID	NR-COM-01-2020-000240.R2
Article Type:	Communication
Date Submitted by the Author:	19-Dec-2019
Complete List of Authors:	Liu, Shihao; National Institute for Materials Science International Center for Nanoarchitectonics Wang, Ying-Chiao; National Institute for Materials Science, International Center for Young Scientists (ICYS) Chang, Chi-Ming; National Chiao Tung University Yasuda, Takeshi; National Institute for Materials Science Fukui, Naoya; The University of Tokyo, Department of Chemistry, Graduate School of Science Maeda, Hiroaki; The University of Tokyo, Department of Chemistry Long, Peihua; The University of Tokyo Nakazato, Kazuo; Nagoya University Jian, Wen-Bin; National Chiao Tung University Xie, Wenfa; Jilin University Tsukagoshi, Kazuhito; National Institute for Materials Science International Center for Nanoarchitectonics, MANA Nishihara, Hiroshi; The University of Tokyo

COMMUNICATION

Solution-processed organometallic quasi-two-dimensional nanosheets as hole buffer layer for organic light-emitting devices

Received 00th January 20xx,
Accepted 00th January 20xx

DOI: 10.1039/x0xx00000x

Shihao Liu[a, f], Ying-Chiao Wang[a], Chi-Ming Chang[b], Takeshi Yasuda[c], Naoya Fukui[d], Hiroaki Maeda[d], Peihua Long[d], Kazuo Nakazato[e], Wen-Bin Jian[b], Wenfa Xie[f], Kazuhito Tsukagoshi[*a], Hiroshi Nishihara[*d]

Two-dimensional (2D) vdW materials have been integrated into optoelectronic devices to achieve exceptional functionality. However, the integration of large-area 2D thin films into organic light-emitting devices (OLEDs) remains challenging because of the finite number of inorganic 2D materials and the high-temperature requirements of their deposition process. The construction of 2D organometallic materials holds immense potential because of their solution synthesis and unlimited structural and functional diversity. Here, we report a facile route using an oil-water interfacial coordination reaction between organic ligands and divalent metal ions to synthesize crystalline quasi-2D organometallic bis(dithiolato)nickel (NiDT) nanosheets with a centimeter scale and a tunable thickness. The NiDT nanosheets can be directly integrated into OLEDs for use as the hole buffer layer and a fluorescent mounting medium without the aid of a transfer process. Moreover, OLEDs with NiDT nanosheets show not only comparable efficiency to conventional OLEDs but also prolonged device lifetime by nearly 2 times. These results open up a new dimension to use quasi-2D organometallic nanosheets as functional layers in large-area organic devices.

Introduction

Atomically flat and dangling-bond-free surfaces of two-dimensional (2D) vdW materials not only provide an ideal interface for efficient carrier injection and transport but also enhance the resistance of 2D vdW materials to interaction with other materials. [1-5] Additionally, 2D vdW materials can also be used as templates for the epitaxial growth of organic semiconductors to control their molecular orientation. [6] Owing to these unique optoelectronic properties, 2D vdW nanosheets are also used to improve device performances of OLEDs. Kim et al. demonstrated that the utilization of transition metal dichalcogenide (TMD) nanosheets as hole injection layers in conventional OLEDs can improve the device stability and change the polarization behavior of emission. [7-8] Pu et al. also reported that OLEDs employing $Ca_2Nb_3O_{10}$ perovskite nanosheet as electron injection layer (EIL) show lower driving voltages compared with the devices with conventional EIL material lithium 8-quinolate. [9]

Even so, although 2D vdW materials have been widely studied for electronic and optoelectronic applications, [10-19] only a few studies have been conducted on the utilization of transition metal dichalcogenides (TMDs) and graphene oxides (GOs) in OLEDs until now. [7, 8, 20-21] Not only does Nature only offer a finite number of inorganic 2D materials, but very few of them have been demonstrated to possess suitable optoelectronic properties which are needed to support efficient OLEDs. These 2D materials are prepared by mechanical cleavage, liquid exfoliation and chemical vapor deposition (CVD) methods. [8] 2D nanosheets prepared by the former two methods are highly fragmented (microsize) and usually integrated into the non-emitting functional layer of OLEDs. Centimeter-scale uniform TMD nanosheets can be produced by the CVD process. [22-26] However, the CVD process has a high-temperature requirement (usually >700 °C), [27] and the ITO substrates required for OLED research cannot survive the harsh environment. Although the synthesized 2D nanosheets can be transferred into OLEDs, they still suffer from film damage because a corrosive solution is used to etch the growth substrate, or some parts of 2D nanosheets easily remain on the carrier polymer. [28]

The incorporation of organic molecules into 2D vdW systems holds an enormous potential since nearly infinite organic molecules can be designed and synthesized with specific functionalities. Motivated by these considerations, we synthesized a bis(dithiolato)nickel (NiDT) nanosheet with a

[a] WPI International Center for Materials Nanoarchitectonics (WPI-MANA) & International Center for Young Scientists (ICYS), National Institute for Materials Science, Tsukuba, Ibaraki, 305-0044, Japan.
[b] Department of Electrophysics, National Chiao Tung University, Hsinchu, 30010, Taiwan, Republic of China.
[c] Research Center for Functional Materials (RCFM), National Institute for Materials Science, Tsukuba, Ibaraki, 305-0047, Japan.
[d] School of Science, The University of Tokyo, Bunkyo, Tokyo, 113-0033, Japan.
[e] School of Engineering, Nagoya University, Chikusa, Nagoya, 464-8603, Japan.
[f] State Key Laboratory of Integrated Optoelectronics, College of Electronic Science and Engineering, Jilin University, Changchun, 130012, People's Republic of China.
† Electronic Supplementary Information (ESI) is available. See DOI: 10.1039/x0xx00.

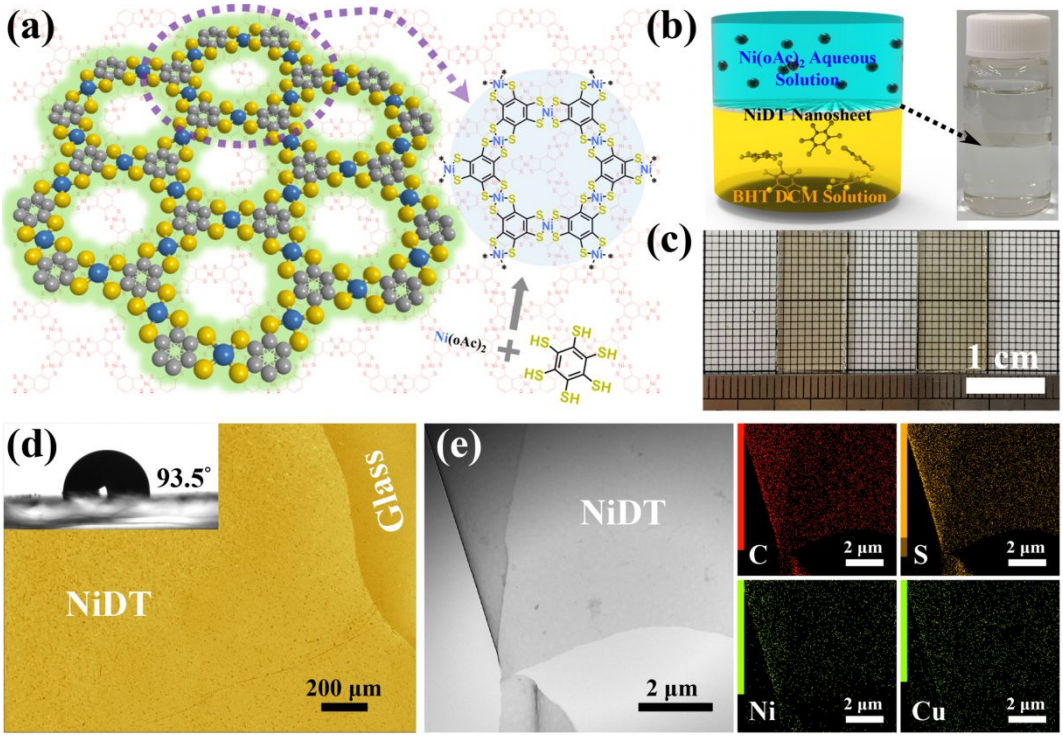

Fig. 1 (a) Schematic illustration and chemical structure of a 2D organometallic NiDT nanosheet (gray, yellow and blue spheres represent carbon, sulfur and nickel, respectively). (b) Schematic illustration and photograph of the water-dichloromethane interface with NiDT nanosheets. (c) Photograph and (d) micrograph of a NiDT nanosheet deposited on a glass substrate; the inset shows a sessile drop of water on the NiDT nanosheet in air. (e) transmission electron microscopy and element mapping image of NiDT nanosheet prepared by dropping reacted solution on copper grid and without any washing process

centimeter scale and a tunable thickness through a liquid/liquid interfacial coordination reaction between benzenehexathiol (BHT) and nickel(II) acetate $Ni(OAc)_2$. NiDT is reported to be oriented in an A-B stacking pattern in the *P6₃/mmc* space group (lattice parameters a=b=1.41 nm and c=0.76 nm), and its electronic conductivity is strongly dependent on the oxidation state. [29-30] The carrier transport dynamics and carrier balance of OLEDs can potentially be regulated when NiDT is integrated. Additionally, NiDT nanosheets can be directly deposited on ITO substrates as functional layers of OLEDs in the fabrication process without any film damage. Then, it is demonstrated that the NiDT nanosheets can be used as a hole buffer layer and a fluorescent mounting medium to achieve efficient OLEDs with extended lifetime. OLEDs with NiDT nanosheets, including polymer devices and small molecule devices, show not only comparable efficiency but also a nearly 2-fold improvement in the device lifetime compared to conventional OLEDs employing PEDOT:PSS as the hole buffer layer.

Results and discussion

2D organometallic materials are emerging due to their structural and functional diversity. [29-31] Figure 1a exhibits a schematic illustration and the chemical structure of a 2D organometallic nanosheet of bis(dithiolato)nickel (NiDT). The NiDT nanosheet is synthesized by a process involving a liquid/liquid interface (Figure 1b) formed by an aqueous layer and an organic layer. The aqueous layer contains $Ni(OAc)_2$ along with NaBr as a charge-compensating agent, and the organic layer consists of a dichloromethane (DCM) solution of benzenehexathiol (BHT). The organic layer with BHT was initially placed in a glass beaker (50 mL) with a diameter of ϕ = 4 cm, followed by coverage with a pure water layer. Then, an aqueous solution containing $Ni(OAc)_2$ and NaBr was gently added into the glass beaker. Under N_2 atmosphere, the material became a transparent solid thin film at the interface after a slow and moderate liquid-liquid interfacial process (Figure 1b).

ITO-coated glass substrates were placed on the bottom of the beaker in advance (Figure S1). After carefully removing the reacted solution, NiDT nanosheets with centimeter scale coverage and uniform morphology (Figures 1c, 1d and S1) were directly deposited on the ITO and then washed thoroughly with pure solvents, including water, ethanol and dichloromethane. The film thickness of the NiDT nanosheets can be tuned by adjusting the reaction time and solution concentration (Figure S2). When 3.3 μmol BHT, 3 μmol NaBr and 24 μmol $Ni(OAc)_2$ were used, a NiDT nanosheet with a 30.5 nm thickness was obtained after a 12 h reaction (Figure S2). In addition, the NiDT nanosheets also exhibit strong hydrophobic properties (water contact angle is 93.5°, Figure 1d), which is beneficial to preventing moisture erosion when NiDT nanosheets are used in OLEDs.

To avoid residual BHT ligands appearing at the interface between the ITO and NiDT nanosheet, $Ni(OAc)_2$ with a much higher mole number (24 μmol) was used to consume all of the BHT (3.3 μmol) here. Figure 1e shows transmission electron microscopy (TEM) and element mapping image of NiDT

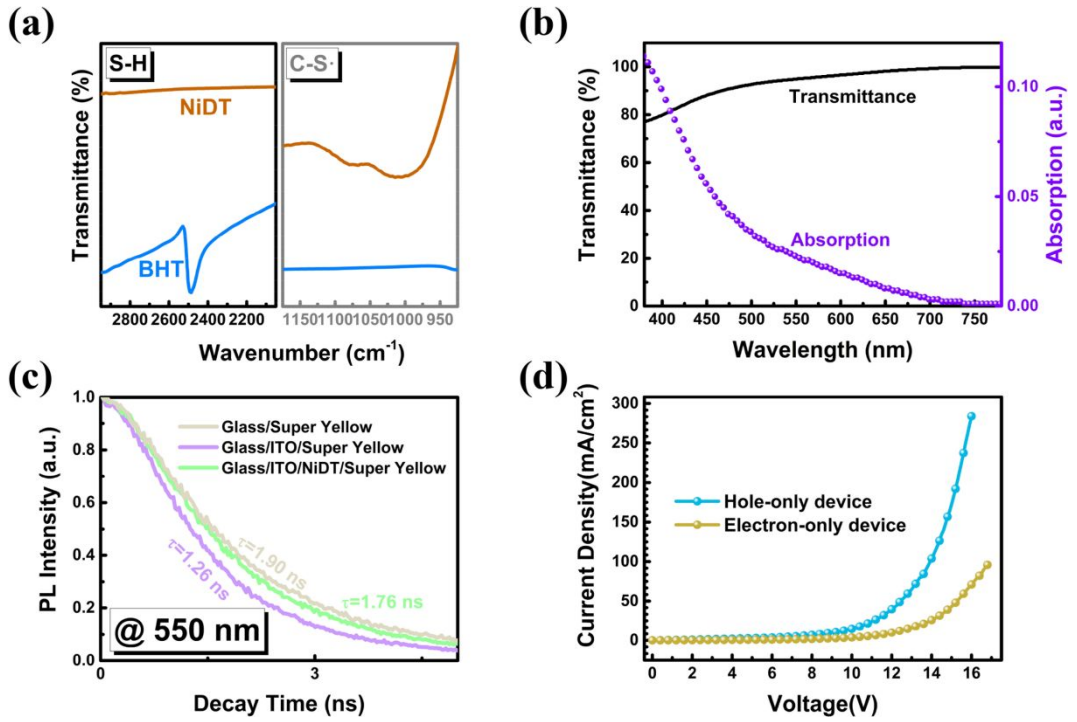

Fig. 2 (a) FTIR transmittance of NiDT nanosheet on ITO substrate and BHT powder. (b) Transmittance and absorption characteristics of a NiDT nanosheet (30 nm). (c) PL transient decay (@550 nm) of Super Yellow on glass, glass/ITO and glass/ITO/NiDT. (d) Current density-voltage characteristics of hole-only and electron-only devices with NiDT nanosheets: hole-only device: ITO/MoO_3 (5 nm)/NiDT (60 nm)/MoO_3 (5 nm)/Al; electron-only device: ITO/LiF (1 nm)/NiDT (60 nm)/LiF (1 nm)/Al.

nanosheet prepared by dropping reacted solution on copper grid and without any washing process. A folded sheet-like morphology of NiDT can be observed with uniform distribution of Ni, S and C, which confirms compositional homogeneity. Besides, S and C mappings possesses much more clear edge compared with Ni element mapping. It indicates nearly all of BHT is used to form the NiDT nanosheet and excess Nickel ions are remained in the reacted solution.

Additionally, comparison of NiDT nanosheets on an ITO substrate and BHT powder in terms of the Fourier transform infrared (FTIR) transmittance spectra is also used to explore the residual situation of BHT, as shown in Figure 2a. BHT has a strong absorption at ~2500 cm^{-1}, corresponding to the S-H stretching vibration, [32] and such a signal does not occur in the NiDT nanosheet on an ITO substrate. Alternatively, the C-S• stretching vibration, corresponding to peaks at 1021 and 1084 cm^{-1}, emerges in the NiDT nanosheet, indicating that all of the thiol groups of BHT participated in the coordination with the Ni ions to form the organometallic nickel bis(dithiolene) structure (Figure 1a). As a result, it is clear that only the NiDT nanosheet was deposited on the ITO substrate, indicating that NiDT nanosheets can be directly integrated into OLEDs using the liquid/liquid interfacial process.

The optical and electrical properties of the NiDT nanosheets, which have significant effects on luminous performances of OLEDs, were also investigated. Figure 2b shows the transmittance and absorption spectra of a NiDT nanosheet with a thickness of 30 nm. The NiDT nanosheet shows high transmittance in the visible wavelength range and strong absorption below 450 nm, indicating that it can facilitate light outcoupling of visible emission from OLEDs and that the NiDT nanosheet has no emission in the visible wavelength range. Since a metal oxide can easily introduce acceptor states for nonradiative transition, [33] the fluorescence quenching effect is observed when Super Yellow is directly deposited on an ITO electrode (Figure 2c). However, as shown in Figure 2c, the fluorescence quenching effect is obviously alleviated after introducing a NiDT nanosheet, indicating that NiDT can serve as a fluorescent mounting medium. This property should be attributed to its metal-organic ligand combination, which reduces the possibility of the presence of dangling bonds. By using MoO_3 as the electron blocking layer and LiF as the hole blocking layer, hole-only and electron-only single carrier devices with NiDT nanosheets were fabricated, respectively. Figure 2d shows their current density-voltage characteristics. Apparently, the NiDT nanosheets prefer hole transport. In addition, according to the reported reference, the onset of oxidation E_{ox}^{on} is equal to 0.21 V. [29] Therefore, the HOMO energy level of the NiDT was estimated to be -4.9 eV from the onset of oxidation E_{ox}^{on} according to the following equation: [34]

$$HOMO = -\left(eE_{ox}^{on} + 4.8(vs.Ag/Ag^{+}) - E_{Fc/Fc+}^{1/2}\right)eV.$$

Thus, its HOMO energy level is also suitable for prompting hole injection from an ITO anode to an organic emitting layer.

Considering the optoelectronic properties of NiDT nanosheets, they were used as hole buffer layers and transport layers to achieve 2D-material hybridized OLEDs. Figure 3a, b shows the device structure and band alignment of a yellow polymer OLED

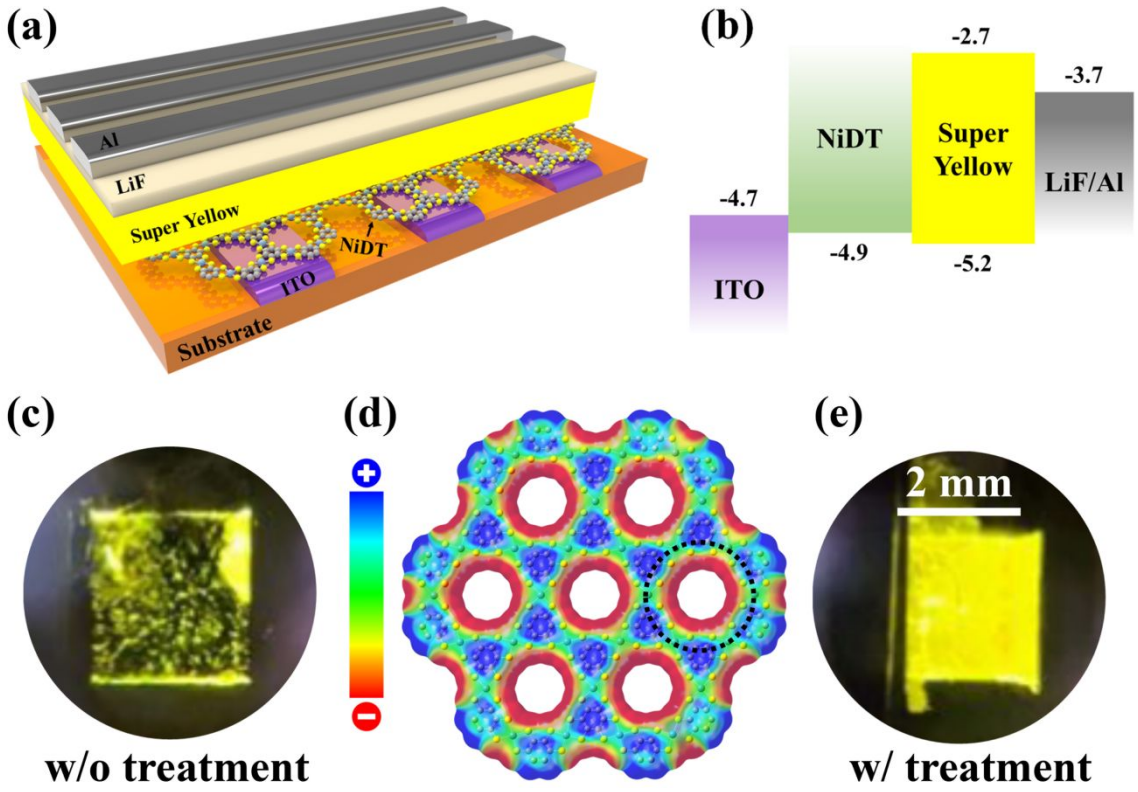

Fig. 3 (a) Device structure and (b) energy level diagram of a yellow polymer OLED with a NiDT nanosheet. (c) Photograph of a yellow polymer OLED with a NiDT nanosheet (w/o any treatment) operating under 3 V. (d) ESP map of nickel bis(dithiolene) units. (e) Photograph of a yellow polymer OLED with a NiDT nanosheet (w/ oxygen/plasma treatment) operating under 3 V.

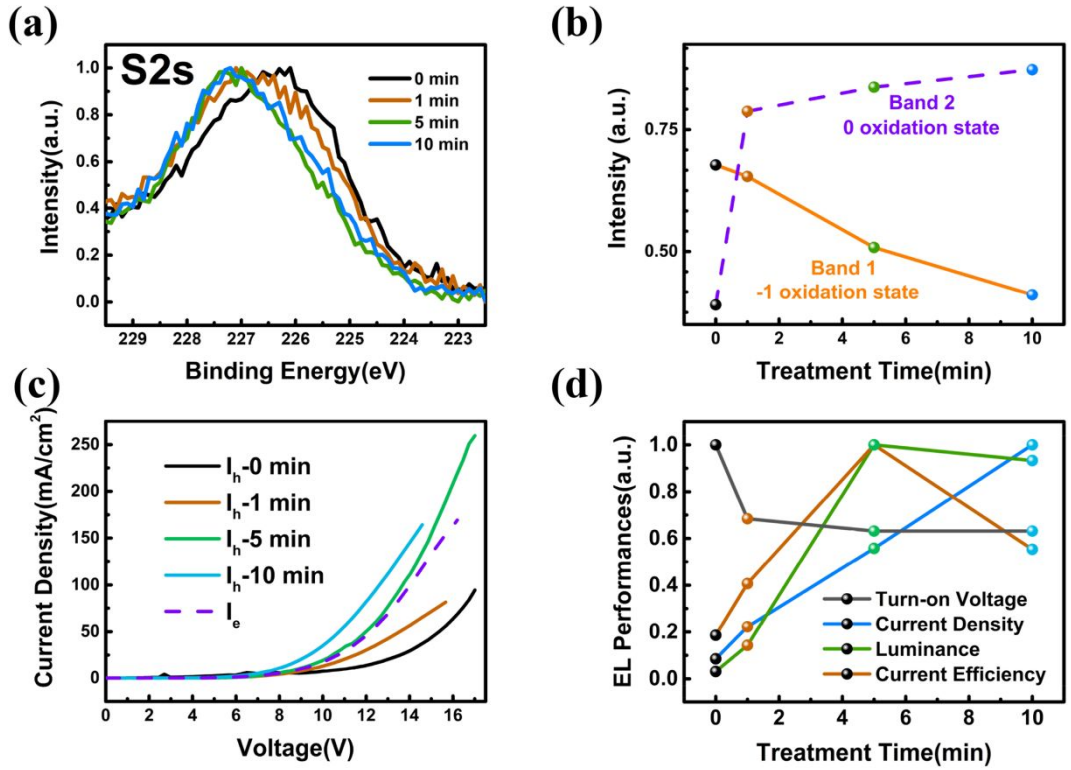

Fig. 4 (a) S 2s XPS spectra and (b) oxidation state variations of NiDT nanosheets after oxygen/plasma treatment. (c) Hole and electron current density of yellow polymer OLEDs with oxygen/plasma-treated NiDT nanosheets. (d) Device performance of yellow polymer OLEDs with oxygen/plasma-treated NiDT nanosheets

with a NiDT nanosheet. The commonly used light-emitting PPV copolymer Super Yellow is used as the emitting layer in the yellow polymer OLEDs here. However, yellow polymer OLEDs with NiDT nanosheets require a high turn-on voltage (3.8 V at 1 cd/m^2) to operate. Figure 3c shows a picture of the yellow polymer OLED with a NiDT nanosheet under a bias voltage of 3 V. Many black spots appear in the operating NiDT, indicating that hole injection from the anode to polymer emitters is insufficient. Because NiDT nanosheets have a suitable HOMO energy level for hole injection (Figure 3b), this problem should be caused by the insufficient hole transport ability of the NiDT nanosheet along the c-axis.

According to the electrostatic potential (ESP) map of nickel bis(dithiolene) units shown in Figure 3d, the conductivity of NiDT nanosheets is relative to the oxidation state of sulfur atoms since areas near sulfur atoms (black dotted circle) are characterized by an abundance of electrons, which is consistent with a previous report. [30] In addition, when the NiDT nanosheets are oxidized by oxygen/plasma treatment, the yellow polymer OLEDs work normally, as shown in Figure 3e. This indicates that the oxidation state of sulfur atoms can be changed by oxygen/plasma treatment, leading to improvement in the hole transport ability of the NiDT nanosheets along the c-axis. As a result, we investigated the influence of oxygen/plasma treatment of the NiDT nanosheets on the device performance of their corresponding yellow polymer OLEDs.

Oxygen/plasma treatment for different times (0, 1, 5 and 10 min) was used to oxidize the NiDT nanosheets. Figure S3 shows the Raman spectra of NiDT nanosheets after oxygen/plasma treatment. Only a small increase in the I_D/I_G ratio is observed in the NiDT nanosheets after 10 min of oxygen/plasma treatment. Generally, the ratio of D and G peaks is used to determine the degree of carbon disorder. [35] Thus, the crystal structure of NiDT nanosheets is not changed by oxygen/plasma treatment. In addition, according to XPS spectra and atomic ratio calculation, the elementary composition of NiDT nanosheet is influenced by oxygen/plasma treatment (Figures S4, S5). After oxygen/plasma treatment, nickel composition decrease and oxygen composition increase sharply. In view of nearly unchanged carbon and sulphur composition, the increase of oxygen composition should be caused by breakage of some unstable coordination bonds and the oxidation of thiol groups. The decrease of nickel composition may be attributed to the formation of nickel oxide on the surface of NiDT nanosheet and its attenuated interaction with NiDT nanosheet. Additionally, the binding energy of the S 2s peak of the NiDT nanosheets increases with treatment time, as shown in Figure 4a. The increase in binding energy is related to variations in the oxidation state of the sulfur atom. [36] According to deconvolution of the S 2s peaks (Figures S6, 4b), the increase in binding energy is caused by an increase of the ratio of 0 to -1 oxidation states.

The variation in the 0/-1 mixed valent oxidation state contributes to the improvement in the hole transport ability of the NiDT nanosheets along the c-axis. Figure 4c shows the hole current density of the devices with NiDT nanosheets treated with oxygen/plasma for different times (0, 1, 5 and 10 min), and the device structures used for the measurements are shown in

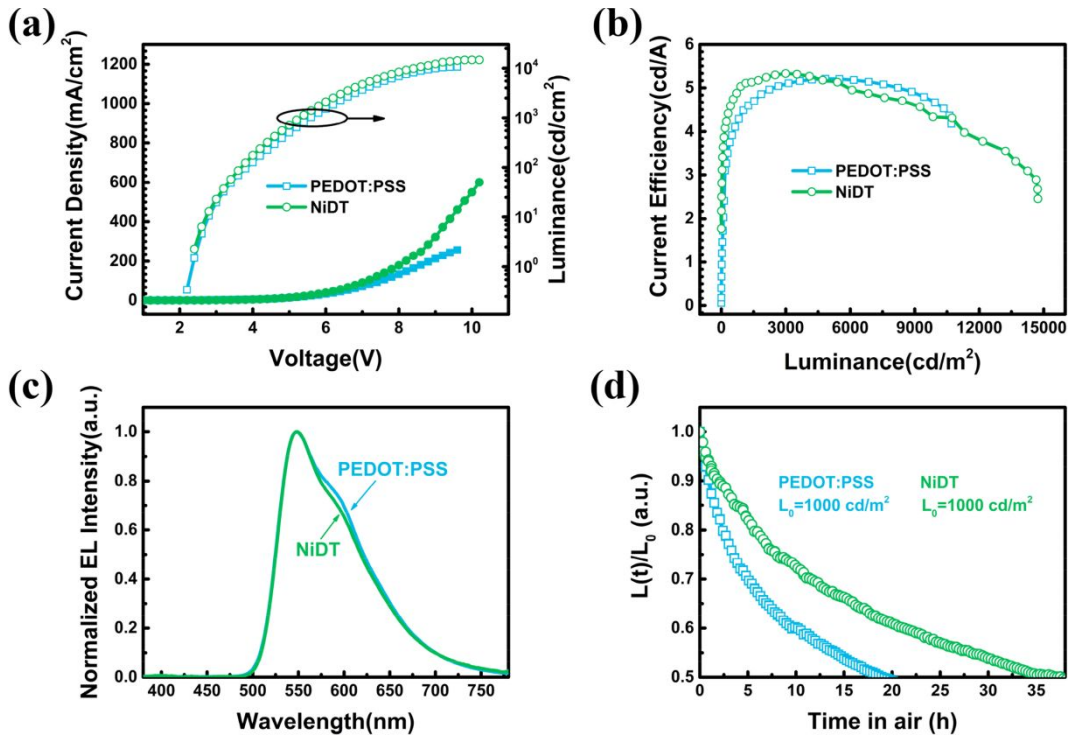

Fig. 5 (a) Current density-voltage-luminance characteristics, (b) current efficiency-luminance characteristics, (c) normalized EL spectra and (d) normalized luminance degradation $L_{(t)}/L_0$ of NiDT and PEDOT:PSS devices with Super Yellow.

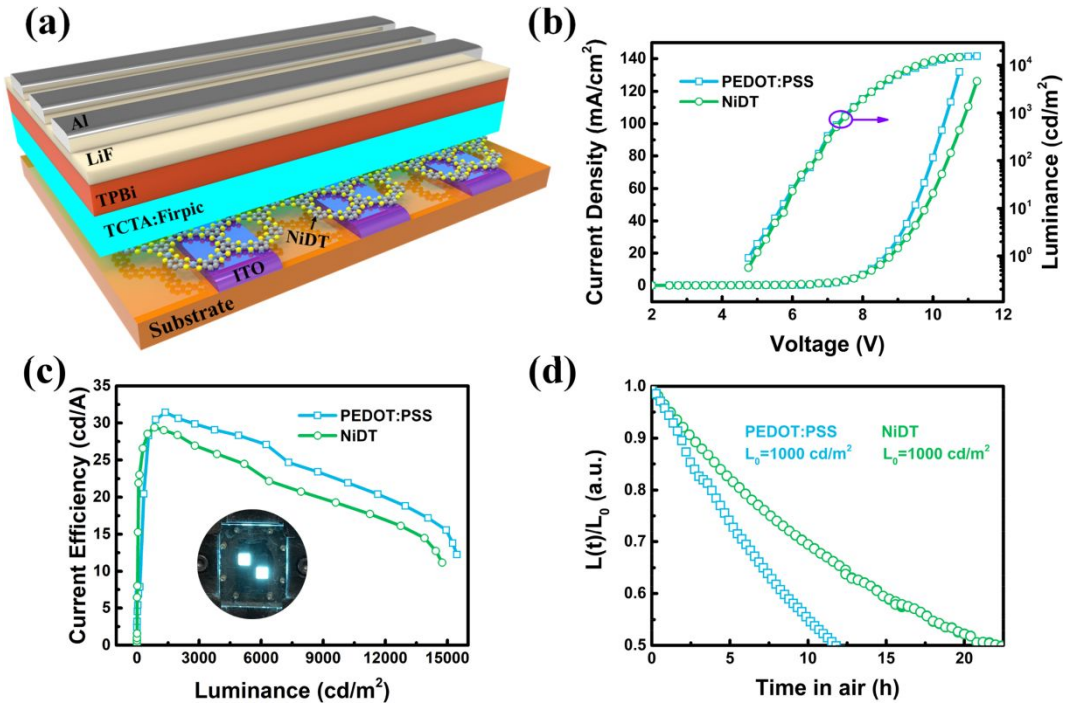

Fig. 6 (a) Device structure of a blue small molecule OLED with a NiDT nanosheet. (b) Current density-voltage-luminance characteristics, (c) current efficiency-luminance characteristics and (d) normalized luminance degradation $L(t)/L_0$ of blue NiDT and PEDOT:PSS devices.

Figure S7. With increasing treatment time, the hole transport ability of the NiDT nanosheets increases. The device performances of NiDT-based OLEDs are also modulated by oxygen/plasma treatment for different times (Figure 4d). The OLED with the NiDT nanosheet treated with oxygen/plasma for 5 min shows the best EL performance because of its best carrier balance between holes and electrons (Figure 4c). The excellent carrier balance also leads to the reduction of exciton–polaron annihilations in OLEDs, which are well known as one main reason for the short operational lifetime of OLEDs. [37] It indicates that the NiDT nanosheet with tunable conductivity has the potential to achieve OLEDs with extended device lifetime.

Figure 5a-c shows the current density-voltage-luminance characteristics, current efficiency-luminance characteristics and normalized EL spectra of a yellow polymer OLED with an oxygen/plasma-treated NiDT nanosheet. For comparison, a conventional yellow polymer OLED employing PEDOT:PSS as the hole buffer layer was also investigated. These devices are marked as the NiDT and PEDOT:PSS devices, respectively. The NiDT device exhibits a maximum luminance of 14730 cd/m^2, a maximum current efficiency of 5.33 cd/A and a maximum external quantum efficiency (EQE) of 4.4 % (Fig. S8), while the values of the PEDOT:PSS device are 10708 cd/m^2, 5.21 cd/A and 4.3%, respectively. Thus, the NiDT device shows comparable EL performances to the conventional PEDOT:PSS device. These devices show the intrinsic yellow emission of Super Yellow with a peak at 550 nm (Figure 5c), except for some differences caused by the influence of the microcavity effect and thickness errors of solution-processed films. [38-39] Meanwhile, the NiDT nanosheet-based OLED has an advantage in device stability. The stabilities of the NiDT and PEDOT:PSS devices were investigated without encapsulation in air under a constant current density of 20 mA/cm^2, and Figure 5d shows the normalized luminance degradation $L(t)/L_0$ of the NiDT and PEDOT:PSS. devices Here, the time elapsed for the brightness to decrease to 50% of the initial value of L_0 under constant current operation is defined as T_{50}. The NiDT device attains T_{50} = 37 h, corresponding to nearly 2 times that of the PEDOT:PSS device. These results indicate that replacing PEDOT:PSS with a NiDT nanosheet as the hole buffer layer could improve the OLED stability because of the hydrophobic, dangling-bond-free properties and tunable conductivity of the NiDT nanosheet.

Finally, since blue small molecule OLEDs suffer from most serious lifetime issue,[37] the NiDT nanosheets are also used to construct efficient blue small molecule OLEDs with extended device lifetime (Figure 6a). Figure 6b, c shows the current efficiency-luminance characteristics of the blue NiDT and PEDOT:PSS devices, and the inset is a picture of the operating device. The maximum current efficiencies of the blue NiDT and PEDOT:PSS devices are 29.4 and 31.4 cd/A, respectively. Their comparable efficiency indicates that the NiDT nanosheet can still efficiently promote carrier injection and confine carriers to the emitting layer consisting of Firpic to form excitons and achieve efficient blue OLEDs. The blue device with the NiDT nanosheet also shows an advantage in device stability. As shown in Figure 6d, the unencapsulated blue NiDT device (@1000 cd/m^2) attains T_{50} = 21 h, corresponding to an 80% improvement from that of the blue PEDOT:PSS device. Additionally, the NiDT nanosheet is also used in a more stable device system for device lifetime measurement, as shown in Fig. S9. The encapsulated NiDT device employing more stable green phosphorescent material tris[2-phenylpyridinato-C^2, N]iridium(III) [Ir(ppy)$_3$] as emitter attains T_{50} = 675 h (@1000 cd/m^2).

Conclusion

A bis(dithiolato)nickel (NiDT) nanosheet with a centimeter scale is synthesized via a liquid/liquid interfacial coordination reaction between BHT and $Ni(OAc)_2$. The thickness of the NiDT nanosheet is tunable by adjusting the reaction time and solution concentration. The crystal quality of the obtained NiDT nanosheets is also revealed by their FTIR spectra, PXRD spectra and TEM images. NiDT nanosheets are also directly integrated as hole buffer layers and fluorescent mounting media in OLEDs without using the transfer method. Oxygen/plasma treatment is further used to modulate the hole transport ability of the NiDT nanosheets along the c-axis. Finally, OLEDs with NiDT nanosheets, including polymer devices and small molecule devices, show not only comparable efficiency but also nearly 2-fold device lifetime compared to conventional OLEDs employing PEDOT:PSS as the hole buffer layer. These results highlight organometallic nanosheets as promising functional materials for organic electronics.

Experimental section

Materials.

$Ni(OAc)_2{\cdot}4H_2O$, NaBr, Super Yellow, poly(3,4-ethylenedioxythiophene)-poly(styrenesulfonate) (PEDOT:PSS), MoO_3, LiF and Al were purchased from Sigma-Aldrich. 4,4',4''-tris(carbazol-9-yl)triphenylamine (TCTA), bis(3,5-difluoro-2-(2-pyridyl)phenyl-(2-carboxypyridyl)iridium(III) (Firpic) and 1,3,5-tris(1-phenyl-1*H*-benzimidazol-2-yl)benzene (TPBi) of OLED grade were purchased from Lumtech Corp. Benzenehexathiol (BHT) was synthesized using the reported method.[40]

Preparation of NiDT nanosheets

Under a nitrogen atmosphere, 2.7 mg BHT powder was added into 30 mL degassed dichloromethane, and 18 mg $Ni(OAc)_2{\cdot}4H_2O$ and 1 mg NaBr were added into 36 mL degassed pure water. Precleaned ITO substrates were placed on the bottom of a beaker (50 mL, ϕ=4 cm) in advance, and then, 10 mL BHT dichloromethane solution, 12 mL degassed pure water and 12 mL aqueous solution containing $Ni(OAc)_2{\cdot}4H_2O$ and NaBr were added into the beaker in sequence. After waiting for a certain reaction time, all the reacted solution was removed, and NiDT-coated ITO substrates were washed thoroughly with water, ethanol and dichloromethane. Finally, the NiDT-coated ITO substrates were heated at 120 °C for 5 min to remove residual solvent.

Preparation of OLEDs

Using the NiDT-coated ITO substrates, Super Yellow films were fabricated by a spin-coating process in a glovebox. The concentration in toluene solution of Super Yellow was 5 mg/mL, and the rotation speed used for spin-coating Super Yellow films was 1200 rpm for 70 nm and 900 rpm for 100 nm. PEDOT:PSS films were fabricated by a spin-coating process with a rotation speed of 5000 rpm in atmosphere and then heated at 120 °C for 10 min to remove residual solvent. The other functional layers, including TCTA:Firpic, TPBi, LiF, MoO_3 and Al, were evaporated via a vacuum thermal evaporation process under high vacuum (~5×10^{-4} Pa) at a rate of 0.1-2 Å s^{-1}, monitored in situ with a quartz oscillator.

Characterization

AFM images were obtained using an AFM5000II/AFM5200S system (Hitachi High-Technologies, Japan) in dynamic mode in atmosphere. Raman spectra were collected with a Nanofinder FLEX Raman system (Tokyo Instruments Inc.) at room temperature. XPS spectra were measured by a PHI 5000 VersaProbe (ULVAC-PHI, INC.), using Al Ka (15 kV, 25 W) as the X-ray source. The XPS spectra were calibrated using the C 1s peak at 284.6 eV. FTIR transmittance spectra were recorded by a Nicolet iS50 at room temperature. Absorption and transmittance spectra were measured by a Shimadzu UV-Visible spectrophotometer UV-2550. The transient PL decay characteristics of Super Yellow were determined using an IHR320 spectrometer (HORIBA, Japan). The current density (J)-voltage (V)-luminance (L) characteristics of the OLEDs were simultaneously measured using a system consisting of an ADCMT 6246 DC source meter (ADC Corporation) and an LS-110 luminance meter (Konica Minolta Japan, Inc.). EL spectra were recorded by an array spectrometer (MCPD-9800-311C, Otsuka Electronics Co., Ltd.).

Conflicts of interest

There are no conflicts to declare.

Acknowledgements

This work was supported by JST-CREST JPMJCR15F2 and JSPS KAKENHI Grant Numbers JP26220801 and JP19H05460 and the National Natural Science Foundation of China (Grant Nos. 61905086 and 61774074). We thank Ms. Chunxiu Zang, Jilin University for the transient PL decay measurement.

References

1 J. Shim, S.-H. Bae, W. Kong, D. Lee, K. Qiao, D. Nezich, Y. J. Park, R. Zhao, S. Sundaram and X. Li, *Science*, 2018, **362**, 665-670.
2 Z. Lin, Y. Liu, U. Halim, M. Ding, Y. Liu, Y. Wang, C. Jia, P. Chen, X. Duan and C. Wang, *Nature*, 2018, **562**, 254.
3 J. Sun, Y. Choi, Y. J. Choi, S. Kim, J. H. Park, S. Lee and J. H. Cho, *Adv. Mater.*, 2019, 1803831.
4 D. Jariwala, T. J. Marks and M. C. Hersam, *Nat. Mater.*, 2017, **16**, 170.
5 D. L. Duong, S. J. Yun and Y. H. Lee, *ACS Nano*, 2017, **11**, 11803-11830.
6 M. Gobbi, E. Orgiu and P. Samorì, *Adv. Mater.*, 2018, **30**, 1706103.
7 G. J. Choi, Q. Van Le, K. S. Choi, K. C. Kwon, H. W. Jang, J. S. Gwag and S. Y. Kim, *Adv. Mater.*, 2017, **29**, 1702598.
8 C. Kim, T. P. Nguyen, Q. V. Le, J. M. Jeon, H. W. Jang and S. Y. Kim, *Adv. Funct. Mater.*, 2015, **25**, 4512-4519.
9 S. Ohisa, T. Hikichi, Y. J. Pu, T. Chiba, J. Kido, ACS Appl. Mater. Inter. 2018, 10, 27885.
10 X. Li, L. Tao, Z. Chen, H. Fang, X. Li, X. Wang, J.-B. Xu and H. Zhu, *Appl. Phys. Rev.*, 2017, **4**, 021306.
11 T. A. Shastry, I. Balla, H. Bergeron, S. H. Amsterdam, T. J. Marks and M. C. Hersam, *ACS Nano*, 2016, **10**, 10573-10579.
12 C. Wang, X. Ren, C. Xu, B. Fu, R. Wang, X. Zhang, R. Li, H. Li, H. Dong and Y. Zhen, *Adv. Mater.*, 2018, **30**, 1706260.
13 T. Wang, K. Andrews, A. Bowman, T. Hong, M. Koehler, J. Yan, D. Mandrus, Z. Zhou and Y.-Q. Xu, *Nano Lett.*, 2018, **18**, 2766-2771.
14 J. Yao and G. Yang, *Small*, 2018, **14**, 1704524.
15 N. Huo and G. Konstantatos, *Adv. Mater.*, 2018, **30**, 1801164.
16 F. Wang, T. Gao, Q. Zhang, Z. Y. Hu, B. Jin, L. Li, X. Zhou, H. Li, G. Van Tendeloo and T. Zhai, *Adv. Mater.*, 2019, **31**, 1806306.
17 T. P. Chen, C. W. Lin, S. S. Li, Y. H. Tsai, C. Y. Wen, W. J.

Lin, F. M. Hsiao, Y. P. Chiu, K. Tsukagoshi and M. Osada, *Adv. Energ. Mater.*, 2018, **8**, 1701722.
18 L. Wang, L. Huang, W. C. Tan, X. Feng, L. Chen, X. Huang and K. W. Ang, *Small Methods*, 2018, **2**, 1700294.
19 D. B. Velusamy, M. A. Haque, M. R. Parida, F. Zhang, T. Wu, O. F. Mohammed and H. N. Alshareef, *Adv. Funct. Mater.*, 2017, **27**, 1605554.
20 R. D. Nikam, P. A. Sonawane, R. Sankar and Y.-T. Chen, *Nano Energy*, 2017, **32**, 454-462.
21 K. Reynolds, J. Barker, N. Greenham, R. Friend and G. Frey, *J. Appl. Phys.*, 2002, **92**, 7556-7563.
22 P. C. Sherrell, P. Palczynski, M. S. Sokolikova, F. Reale, F. M. Pesci, M. Och and C. Mattevi, *ACS Appl. Energ. Mater.*, 2019, **2**, 5877-5882.
23 H. Yu, M. Liao, W. Zhao, G. Liu, X. Zhou, Z. Wei, X. Xu, K. Liu, Z. Hu and K. Deng, *ACS Nano*, 2017, **11**, 12001-12007.
24 Z. Dai, Z. Wang, X. He, X. X. Zhang and H. N. Alshareef, *Adv. Funct. Mater.*, 2017, **27**, 1703119.
25 H. D. Phan, Y. Kim, J. Lee, R. Liu, Y. Choi, J. H. Cho and C. Lee, *Adv. Mater.*, 2017, **29**, 1603928.
26 L. Zhan, W. Wan, Z. Zhu, Y. Xu, T.-M. Shih, C. Zhang, W. Lin, X. Li, Z. Zhao and H. Ying, *J. Phys. Chem. C*, 2017, **121**, 4703-4707.
27 A. Mitioglu, K. Galkowski, A. Surrente, L. Klopotowski, D. Dumcenco, A. Kis, D. Maude and P. Plochocka, *Phys. Rev. B*, 2016, **93**, 165412.
28 L. Tao, K. Chen, Z. Chen, W. Chen, X. Gui, H. Chen, X. Li and J.-B. Xu, *ACS Appl. Mater. Interfaces*, 2017, **9**, 12073-12081.
29 T. Kambe, R. Sakamoto, K. Hoshiko, K. Takada, M. Miyachi, J.-H. Ryu, S. Sasaki, J. Kim, K. Nakazato and M. Takata, *J. Am. Chem. Soc.*, 2013, **135**, 2462-2465.
30 T. Kambe, R. Sakamoto, T. Kusamoto, T. Pal, N. Fukui, K. Hoshiko, T. Shimojima, Z. Wang, T. Hirahara and K. Ishizaka, *J. Am. Chem. Soc.*, 2014, **136**, 14357-14360.
31 R. Matsuoka, R. Sakamoto, K. Hoshiko, S. Sasaki, H. Masunaga, K. Nagashio and H. Nishihara, *J. Am. Chem. Soc.*, 2017, **139**, 3145-3152.
32 K. Ray, T. Weyhermüller, F. Neese and K. Wieghardt, *Inorg. Chem.*, 2005, **44**, 5345-5360.
33 J. Maaβ, M. Wollenhaupt, H. Abrens, P. Fröbel and K. Bärner, *J. Lumin.*, 1994, **62**, 95-100.
34 H. Wei, H. Lu, T. Fang and Z. Bo, *Sci. China Chem.*, 2015, **58**, 286-293.
35 D.-w. Kim, O. L. Li and N. Saito, *Phys. Chem. Chem. Phys.*, 2015, **17**, 407-413.
36 D. Sellmann, H. Binder, D. Häußinger, F. W. Heinemann and J. Sutter, *Inorg. Chim. Acta*, 2000, **300**, 829-836.
37 J. Lee, C. Jeong, T. Batagoda, C. Coburn, M. E. Thompson and S. R. Forrest, *Nat. Commun.*, 2017, **8**, 15566.
38 S. Hofmann, M. Thomschke, B. Lüssem and K. Leo, *Opt. Express*, 2011, **19**, A1250-A1264.
39 S. Liu, J. Liu, X. Wen, Y. Liu, Z. Chen, Y. Yin, L. Zhang and W. Xie, *Opt. Lett.*, 2013, **38**, 1742-1744.
40 J. A. Harnisch and R. J. Angelici, *Inorg. Chim. Acta*, 2000, **300**, 273-279.

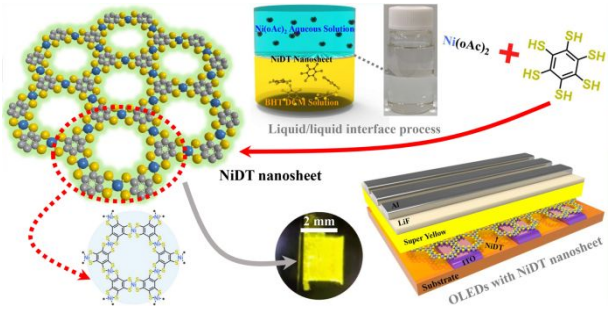

Quasi-2D organometallic bis(dithiolato)nickel nanosheet is successfully integrated into organic light-emitting devices to achieve extended device lifetime.